RESEARCH ARTICLE

VG161 activates systemic antitumor immunity in pancreatic cancer models as a novel oncolytic herpesvirus expressing multiple immunomodulatory transgenes

Yinan Shen[1,2] | Wei Song[2] | Danni Lin[1,2] | Xiaozhen Zhang[1,2] | Meng Wang[1,2] |
Yuwei Li[1,2] | Zifan Yang[2] | Sida Guo[3] | Zijun Wang[3] | Jianpeng Sheng[2] |
Yanal Murad[4] | Jun Ding[5] | Yufeng Lou[3] | Xinping Pan[6] | Zongsong Wu[5] |
Ronghua Zhao[4,5,6] | Weiguo Jia[4,5,6] | Xueli Bai[1,2] | Tingbo Liang[1,2]

[1]Department of Hepatobiliary and Pancreatic Surgery, The First Affiliated Hospital , Zhejiang University School of Medicine, Hangzhou, China

[2]Zhejiang Provincial Key Laboratory of Pancreatic Disease, The First Affiliated Hospital, Zhejiang University School of Medicine, Hangzhou, China

[3]Center for Innovation & Translational Medicine, The First Affiliated Hospital, Zhejiang University School of Medicine, Hangzhou, China

[4]Virogin Biotech Canada Ltd., Vancouver, British Columbia, Canada

[5]Shanghai Virogin Biotech Co. Ltd., Shanghai, China

[6]CNBG-Virogin Biotech (Shanghai) Co. Ltd., Shanghai, China

Correspondence

Tingbo Liang, Department of Hepatobiliary and Pancreatic Surgery, The First Affiliated Hospital, Zhejiang University School of Medicine, 79 Qingchun Road, Hangzhou 310006, Zhejiang Province, China.
Email: liangtingbo@zju.edu.cn

Abstract

The VG161 represents the first recombinant oncolytic herpes simplex virus type 1 carrying multiple synergistic antitumor immuno-modulating factors. Here, we report its antitumor mechanisms and thus provide firm theoretical foundation for the upcoming clinical application in pancreatic cancer. Generally, the VG161-mediated antitumor outcomes were analyzed by a collaboration of techniques, namely the single-cell sequencing, airflow-assisted desorption electrospray ionization-mass spectrometry imaging (AFADSI-MSI) and nanostring techniques. In vitro, the efficacy of VG161 together with immune checkpoint inhibitors (ICIs) has been successfully shown to grant a long-term antitumor effect by altering tumor immunity and remodeling tumor microenvironment (TME) metabolisms. Cellular functional pathways and cell subtypes detected from patient samples before and after the treatment had undergone distinctive changes including upregulated CD8+ T and natural killer cells. More importantly, significant antitumor signals have emerged since the administration of VG161 injection. In conclusion, VG161 can systematically activate acquired and innate immunity in pancreatic models, as well as improve the tumor immune microenvironment, indicative of strong antitumor potential. The more robusting antitumor outcome for VG161 monotherapy or in combination with other therapies on pancreatic cancer is worth of being explored in further clinical trials.

KEYWORDS

clinical and translational science, immune microenvironment, oncolytic virus, pancreatic cancer, synergistic agents

1 | INTRODUCTION

Pancreatic cancer is predicted to become the second leading cause of cancer-related deaths by 2030 in the United States. [1] The 5-year survival rate for pancreatic cancer is 8%,[2] calling for the need for more effective treatments. Oncolytic viruses (OVs) selectively destroy tumor cells, while causing virtually negligible damage to normal cells. A diverse range of OVs have shown efficacy in preclinical studies.[3–5] To date, approximately 30 types of OVs have entered clinical trials around the world. Unfortunately, it still lacks a satisfying therapeutic strategy for the oncolytic virus as a monotherapy or in combination with other treatments in current pancreatic cancer clinic trials. Even though H101 has gained regulatory approval, it has to be combined with other treatments to reach an effective outcome, for its immunoregulatory role in cancer treatment is still limited. The other approvedoncolytic herpes simplex virus type 1, talimogene laherparepvec (T-VEC) expresses cytokine granulocyte-macrophage colony-stimulating factor (GM-CSF),[6–10] has obtained a favorable effect with programmed cell death protein 1 (PD-1) monoclonal antibody therapy.[11] However, recent studies have shown that GM-CSF induces the proliferation of myeloid suppressor cells (MSCs) in neoplasms, facilitating immune suppression and immune escape.[12–14] Therefore, a novel immune-boosted oncolytic virus is urgently required.

Human antitumor immunity primarily consists of adaptive and innate immune responses. A cancer-immunity cycle (CIC) is formed in relation to adaptive antitumor immunity and a cancer-natural killer cell immunity cycle (CNIC) is involved in innate antitumor immunity.[15,16] The immune response is often rapid, durable, adaptable, and the immune cells involved could be self-propagating.[15,17] With each revolution of the cycle, renascent antitumor immune responses rely on neoantigen spreading.[18] In recent years, natural killer (NK) cells and macrophages have drawn increasing attention in innate immunity and have been shown to play pivotal roles in antitumor immunity. In particular, NK cells appear to enhance the effect of immune checkpoint inhibitor (ICI) treatment in the CNIC. It indicates the significance of NK-mediated efficacy and ICIs when considering the induction of optimal antitumor outcomes. An ideal antitumor immunotherapeutic drug may ideally consider both CIC and CNIC, refraining from disruption of the cycle.

VG161 is a herpes simplex virus containing the genes encoding interleukin (IL)-12, IL-15, IL-15 receptor alpha subunit isoform 1 (IL-15RA), and a fusion protein (TF-Fc) capable of blocking the PD-1/PD-L1 interaction. In addition, VG161 has a deletion in the viral gene encoding ICP34.5 as a safety measure to abrogate neurovirulence. Unlike T-VEC, VG161 remains the original ICP47 functioning for its role in enhancing virion persistence to extend the window of payload expression. In a previous study, a cooperative immunostimulatory effect was identified between IL-12, IL-15, and a PD-L1 blocker.[19] In this study, by utilizing a multiplicity of pancreatic cancer mouse models, we attempted to scrutinize the antitumor mechanisms of VG161 in preclinical studies and, thus, to extend the future clinical applications of OVs in pancreatic cancer therapeutics.

2 | MATERIALS AND METHODS

2.1 | Oncolytic virus

The VG161, VG160, and mVG161 constructions were performed as described previously.[19] Herpes simplex virus type 1 (HSV-1) strain 17 provides the backbone for the construction of all the mentioned recombinant viruses in which ICP34.5 was deleted. An expression cassette for secretable PD-L1 blocking peptide, a fusion protein TF was conjugated to human IgG4 Fc (TF-Fc), and genes encoding human IL-12, IL-15, and IL-15 receptor alpha subunit isoform 1 (IL-15RA) were constructed into HSV-1, termed hVG161(VG161). In contrast, VG160 neither express human IL-12, IL-15, IL-15RA, nor the PD-L1 blocking peptide. The mVG161 was identical to VG161 apart from the substitution of mouse IL-12 for human IL-12 and the presence of a mouse-specific version of the PD-L1 blocker conjugated with mouse IgG1 Fc.

2.2 | Cell culture

The information of human cell lines and mouse tumor lines used in this study were detailed in the Supporting Information. All cell lines were verified to be mycoplasma free by polymerase chain reaction (PCR).

2.3 | Three-dimensional (3D) cell culture and virus infection

After autoclaving, 1% molten agarose dissolved in phosphate buffer saline was allowed to cool to about 60°C, and 50 µl agarose solution was added to each well in 96-well plates. After the agarose had solidified, a total of 5000 cells were plated onto the agarose wells. After culturing for 6 days, 3D cells had formed, and the indicated viruses were added. Images of the 3D cells were observed at 24, 96, and 168 h with an optical microscope (DM2500 LED; Leica).

2.4 | Mouse tumor models

The mouse tumor models information and detailed operation were described in the Supporting Information. The drug was administered by intratumoral injection, which is the most commonly used approach.[7–11] All animal experiments were approved by the Ethics Committee of the First Affiliated Hospital, School of Medicine, Zhejiang University. All animal care and handling procedures were performed normatively and humanely.

2.5 | Viral oncolysis

Cells were seeded into a 96-well plate and infected with the indicated viruses at an multiplicity of infection (MOI) of 0.01, 0.1, 1, and 10. Cell viability assays were scored 24–96 h later using Cell Counting

Kit-8 (K1018; APExBIO). The absorbance for each well was read at 450 nm by using a microplate reader (SpectraMax i3x; Molecular Devices).

2.6 | Viral replication

Cells were seeded into a six-well plate and infected with the indicated viruses at an MOI of 1. The cells were harvested at 24, 48, and 72 h postinfection. After three freeze and thaw cycles, the viruses were separated and titrated in Vero cells using a standard plaque assay in six-well plates.

2.7 | Flow cytometry analysis of tumor infiltrating lymphocytes

The cell preparation and staining procedures, and the information of antibodies were described in the Supporting Information. All samples were acquired on a BD LSRFortessa instrument and the data was analyzed using FlowJo V10 software.

2.8 | Biodistribution analysis

Biodistribution analysis of VG161 was performed in a nude mouse model implanted with BxPC3 cells. In brief, 1×10^7 PFU of VG161 was intratumorally injected into mice bearing the BxPC3 tumor, and different tissues, which include the kidney, lung, spleen, liver, heart, noninjected tumor, and injected tumor were harvested at 0, 0.5, 1, 2, 3, and 7 days. DNA was extracted with a DNeasy Blood and Tissue Kit (69504; Qiagen), and the viral copies were quantified by qPCR to the codon optimized IL-15RA1 gene, which expression is unique to VG161. The VG161 copy numbers were calculated per μg of genomic DNA. The information of primers and probes were described in the Supporting Information.

2.9 | Mouse interferon γ (IFN-γ) enzyme-linked immunosorbent spot (ELISpot) assay

Splenocytes were harvested from treated mice at the indicated time points. The cells were then subjected to an ELISpot assay using a Mouse Interferon-γ (IFN-γ) ELISpot kit (221005; Dakewe) according to the manufacturer's instructions. Briefly, the splenocytes (1×10^5 cells/well) were incubated in a 96-well plate in the presence of precoated anti-IFN-γ antibody at 37°C overnight with mouse pancreatic cancer cell lines (KPC) (5×10^4 cells/well). Biotinylated secondary antibody, horse radish peroxidase-conjugated streptavidin, and 3,3', 5,5"-tetramethylbenzidine substrate were subsequently added in sequence. The results are expressed as the number of positive spots in each well.

2.10 | Single-cell RNA sequencing

KPC tumors were treated with a vehicle, VG160, or VG161 (1×10^7 PFU) intratumorally, and subsequently harvested after 3, 7, and 22 days. The tumors were dissociated into a single-cell suspension, which was loaded into the Chromium microfluidic with V5 chemistry and barcoded with a 10× Chromium Controller (10× Genomics). Reverse transcription was performed on RNA acquired from the barcoded cells. The library preparation was constructed with reagents from a Chromium Single Cell V5 reagent kit (10× Genomics) in accordance with the manufacturer's protocol. The libraries were sequenced on an Illumina sequencing platform (Novaseq. 6000; Illumina) by OE Co., Ltd.

2.11 | Sample preparation and airflow-assisted desorption electrospray ionization-mass spectrometry imaging (AFADSI-MSI) analysis

Fresh tumor tissues were embedded in paraffin, cut into 10 μm sections with a Leica CM1950 cryostat microtome at −20°C. All tissue sections were stored at −80°C until dried in a vacuum container for 1 h before AFADSI-MSI analysis. Serial tissue sections were heated at 68°C for 1 h. After dewaxing, the tissue sections were stained with hematoxylin and eosin (H&E).

Spatial multiomics analyses were performed on an AFADESI-MSI platform, which consists of a Q-Orbitrap mass spectrometer (Orbitrap Fusion Lumos, Thermo Fisher Scientific) and an AFADESI ambient ion source by LM CO., Ltd. In brief, the tissue sections were fixed on an electrical moving stage, which moved at a horizontal rate of 200 μm/s with a 200 μm vertical step. The spectra were acquired in both positive and negative-ion mode. The extracting gas flow was 45 L/min, and the capillary temperature was 350°C. Data were analyzed using Xcalibur software (Version 2.2; Thermo Fisher Scientific).

2.12 | Statistical analysis

All statistical analyses were performed using GraphPad Prism software version 7.0. Data were analyzed using unpaired Student's t-tests. p values less than 0.05 were considered to be statistically significant (*$p < 0.05$; **$p < 0.01$; and ***$p < 0.001$).

3 | RESULTS

3.1 | VG161 induces oncolytic cytotoxicity in tumor cells and antitumor effect in a pancreatic cancer animal model

CCK8 assay results showed that VG161 exhibited certain cytotoxicity in different tumor cell lines and was positively correlated with MOI (Figure 1A). Interestingly, the flow cytometry results showed that
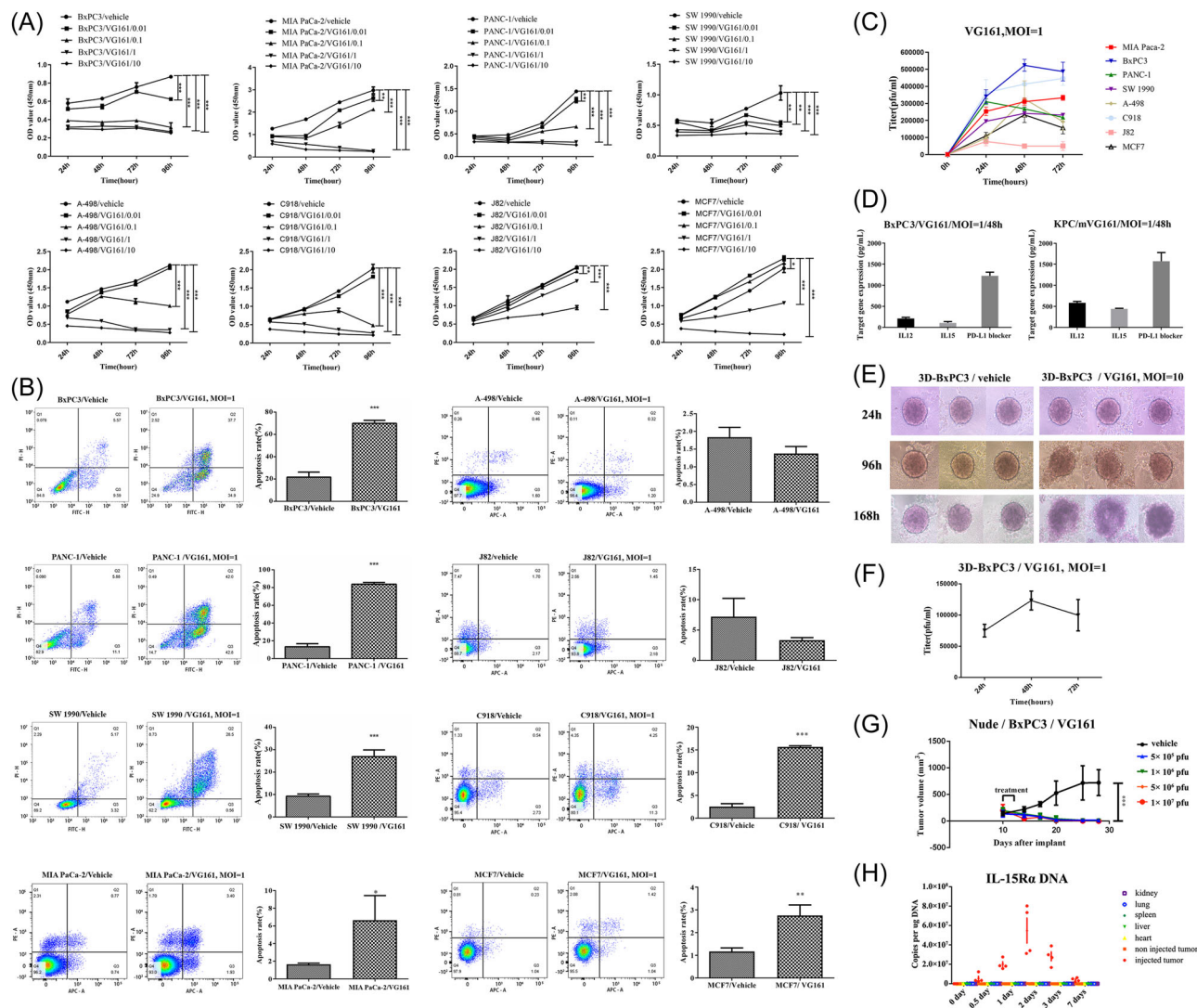
FIGURE 1 VG161 induces antitumor effect in tumor cells and a pancreatic cancer animal model. (A) The cytotoxicity of VG161 was evaluated in a variety of human cancer cell lines at 24, 48, 72, and 96 hpi with an infection multiplicity of infection (MOI) of 0.01, 0.1, 1, and 10. (B) The proapoptotic effects of VG161 were evaluated in a variety of human cancer cell lines at 48 hpi (MOI of 1) by flow cytometry. (C) Cells infected as in (A) were harvested at the indicated time points and the intracellular viral titers were determined using a standard plaque assay. (D) VG161 armed exogenous gene expression in BxPC-3 and KPC cells were quantified by Enzyme-linked immuno sorbent assay (ELISA). (E) The cytotoxicity of VG161 was observed in a three-dimensional (3D) pancreatic cancer model of BxPC3 at indicated time points by scanning confocal laser microscopy. (F) The intracellular viral titers of 3D-BxPC3 cells infected with VG161 were determined at indicated time points using a standard plaque assay. (G) Nude mice were subcutaneously implanted with 2×10^6 BxPC3 human pancreatic cancer cells into the lower left flank, followed by five continuous days intratumoral injection of either vehicle control or different dosages of VG161 ($n = 5$). Tumor volumes were then monitored at indicated days after implantation. (H) Nude mice bearing bilateral BxPC-3 tumors were injected intratumorally with 1×10^7 PFU/mouse of VG161($n = 5$) and were euthanized at different time points. The tissue-specific distribution of VG161 were detected by qPCR targeted at interleukin (IL)-15Rα gene carried by oncolytic virus. Data are shown as the mean ± SEM. Stats: Data were analyzed using an unpaired Student's t-test, $^*p < 0.05$; $^{**}p < 0.01$; $^{***}p < 0.001$.

VG161 could promote apoptosis (Figure 1B) in all pancreatic cancer cell lines. We subsequently detected the ability of VG161 to replicate in different tumor cell lines with plaque assays. It suggested that VG161 replicates effectively in all tumor cell lines (Figure 1C). Next, we examined the expressions of exogenous genes encoded by VG161 in (KPC) and human pancreatic cancer cells (BxPC-3) by enzyme-linked immuno sorbent assay, and found that the exogenous

genes IL-12, IL-15/IL-15Rα, and PD-L1 blocker carried by VG161 were stably expressed in both KPC and BxPC-3 (Figure 1D).

In vitro, the 3D organoid of pancreatic cancer spheroids was constructed to imitate the in vivo behaviors of pancreatic neoplasms in terms of the phenotype and genotype. Under microscopic observations, we found that the organoid cultivated using BxPC3 cells gradually collapsed and decomposed (Figure 1E) due to the

oncolytic activity of VG161. The lysing capability of VG161 was effectively replicated in all organoids (Figure 1F), which was further validated by plaque assays. In vivo, the antitumor effect was confirmed at all doses of VG161 administered in pancreatic cancer nude mouse model (Figure 1G). Furthermore, we measured the DNA copy numbers of IL-15Rα in the mice administered with single dose of VG161 at various time points. The results showed that the DNA copy number of IL-15Rα was significantly higher only in the tumor injection site and peaked at 48 h (Figure 1H). The organ injury indexes (e.g., alanine transaminase [ALT], creatinine [CR], and lactic dehydrogenase [LDH]) were measured in the peripheral blood of the mice. All the indexes were found to increase transiently after injection, peaked at 48 h, and quickly returning to the baseline (Supporting Information: Figure 1A). Finally, the organs were collected for HE staining. The histological analysis revealed that VG161 caused no damage to normal tissue cells (Supporting Information: Figure 1B), suggesting that VG161 represents a good safety profile in nonimmunized mice with anticancer ability.

3.2 | VG161 expressed payloads inducing strong antitumor immune responses

To better scrutinize the ability of VG161 in activation of antitumor immunity in vivo, we employed an immune-competent mouse model harboring KPC cells. In vitro mVG161 exhibited cell killing effect (Supporting Information: Figure 2A) on KPC cells at an MOI of 10 or higher in a CCK8 assay. The plaque assays suggested that mVG161 could replicate effectively in KPC cells (Supporting Information: Figure 2B). In vivo, the tumor growth in mice was significantly inhibited (Supporting Information: Figure 2C). CD8+T cell markers, Tumor necrosis factor-α, granzyme B, and IFN-γ were upregulated compared to those exhibited in the vehicle group (Supporting Information: Figure 2D), examined by flow cytometry. Here, we confirmed that KPC cells reacted to OV treatments favorably in the perspective of immunogenicity phenotype in vivo and, thus, the tumor-bearing mouse established with KPC implantation would represent a viable immune model for our drug analysis.
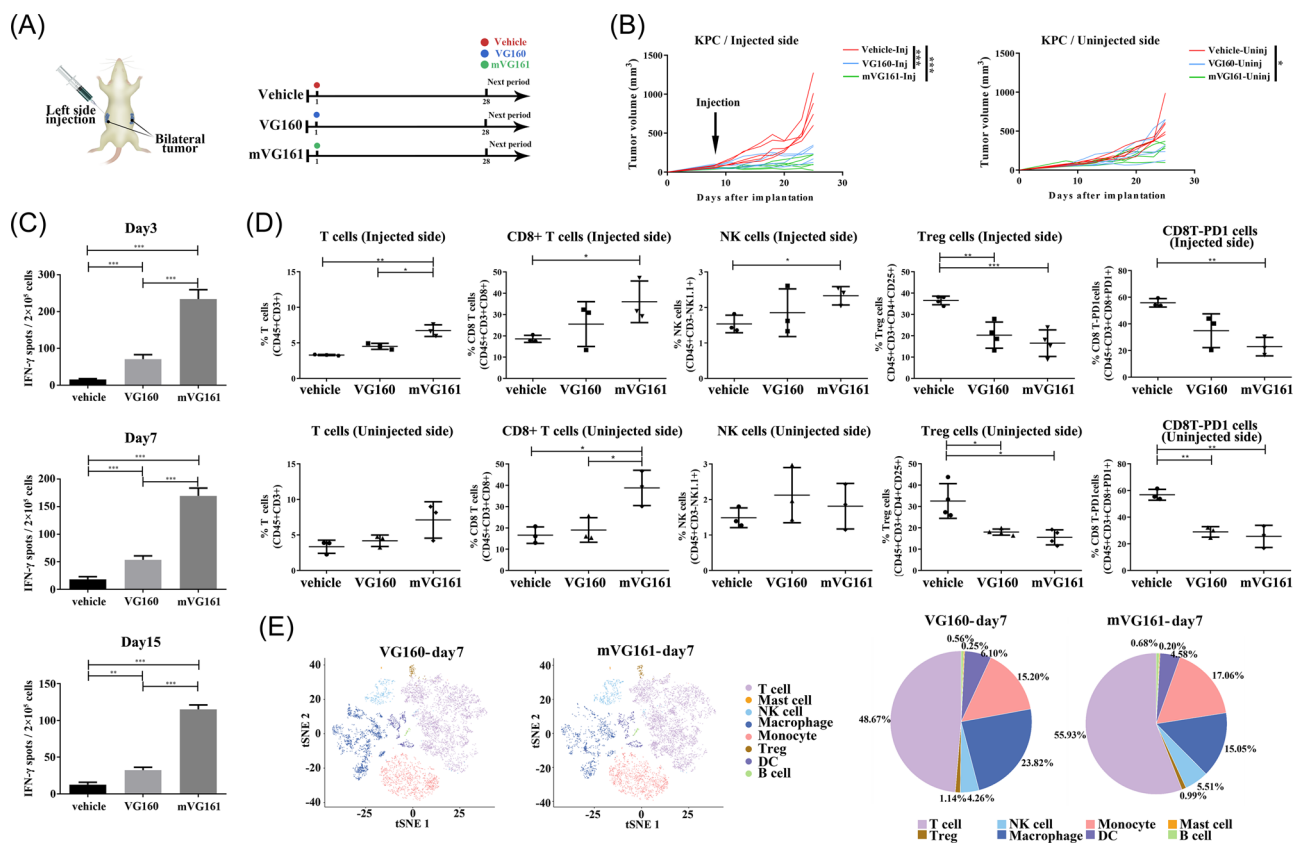
FIGURE 2 VG161 armed exogenous gene suppresses the growth of pancreatic cancer in a C57BL/6 mouse model by stimulating antitumor immunity. (A) C57BL/6 mice bearing bilateral KPC tumors were intratumorally injected into the left side with 1×10^7 PFU/mouse of VG160, mVG161, or vehicle control (n = 5). (B) Tumor growth of individual injected tumors and uninjected distant tumors. (C) The interferon (IFN)-γ exspression level of spleen was detected by ELISpot at indicated time. (D) Tumor infiltration of immune cells in the injected tumors and uninjected distant tumors was assessed by flow cytometry. (E) t-distributed stochastic neighbor embedding (t-SEN) analysis of tumor cells from VG160 and mVG161-injection side (left). Each cell population were determined as the percentage of the total CD45+ cells (right). Composition of vehicle: 50 mM Tris-HCl, 150 mM NaCl, 5% glycerol. Data are shown as the mean ± SEM. Experiments B-D were repeated at least twice. Stats: Data were analyzed using an unpaired Student's t-test, *p < 0.05; **p < 0.01; ***p < 0.001.

Next, to further verify whether the exogenous genes carried by VG161 could deliver an enhanced antitumor activity, we used the VG160 backbone virus as the positive control group and vehicle as the negative control group. To this end, KPC tumors were implanted to both flanks of C57BL/6 mice (4×10^5 cells at each site). After tumor formation, the left tumor was treated with intratumoral injection with either VG160 or mVG161. The results showed that both mVG161 and VG160 significantly inhibited tumor growth at the injection side. As expected, the tumor growth was inhibited by mVG161 to a greater extent than VG160 (Figure 2B). In addition, significant tumor suppression at the opposite uninjected side was only observed in the mVG161 group (i.e., abscopal effect). At Days 3, 7, and 15 following the administration, spleen samples were obtained for ELISpot detection. The results revealed that IFN-γ was significantly upregulated (Figure 2C) in the mVG161 group. Bilateral tumors were also collected from the mice at Day 7 after administration for flow cytometry analysis (Figure 2D). A significantly enhanced infiltration of CD8+ T cells was observed in bilateral tumors in both VG160 and mVG161 groups, with a slightly higher degree of infiltration observed in the mVG161 group. Interestingly, the infiltration of CD8+ T cells in the uninjected tumors in the mVG161 group was significantly higher than that in other groups. These findings help to explain the observation of "abscopal effect" brought about by mVG161. In addition, the number of NK cells alongside with the injection side was increased at Day 7 following the administration of mVG161. This can be explained by the upregulation of NK cells due to enhanced IL-15/IL-15RA signaling. What is more noteworthy is that the ratio of CD8+/PD-1+ T cells was significantly suppressed in bilateral neoplasms in mVG161 group. This provides us the clue that the PD-L1 blocker carried by mVG161 have played a pivotal role in ameliorating the immune-suppressive environment.

Previous studies have shown that OVs can induce changes in the tumor immune microenvironment.[19–22] To confirm the effects of the exogenous genes carried by VG161, we performed single-cell sequencing on the tumor from the injection side of the mice at Day 7 postadministration. We first used an unsupervised clustering data analysis to separate the CD45+ cells into distinct groups of immune populations. These immune populations were then further classified based on the expression of known markers for each population (Figure 2E). The results showed that mVG161 represents a stronger correlation with positive immune responses than VG160. More macrophages were detected in the VG160 group. Furthermore, we found an incresence of infiltrated T cells in the tumors of individuals receiving mVG161. This can be attributed to increased immune cell recruitment by the viral infection and stimulated T-cell proliferation through the expression of IL-12/IL-15. Moreover, the mVG161-infected tumors displayed an influx of new, effector-like CD8+ T cells, NK cells, and monocytes. There was also a proportional loss of dysfunctional or suppressive cells, such as Tregs and tumor-associated macrophages compared to the VG160-infected tumors.

3.3 | Impact of VG161 on tumor metabolisms in TME

Since there are few research studies that have evaluated the regulations in tumor metabolisms following the OV treatment, therefore, we collected subcutaneous tumor samples of mice at Day 3 after receiving the VG160 or mVG161 treatment and compared with the vehicle group using AFADSI-MSI technology. The results showed that the metabolic changes after receiving the VG160 or mVG161 were similar. Specifically, some amino acid metabolic pathways (e.g., beta-alanine metabolism, arginine and proline metabolism, and thermogenesis) were significantly upregulated, whereas other pathways (e.g., arachidonic acid metabolism, linoleic acid metabolism, and neuroactive ligand-receptor interaction) were downregulated (Figure 3A). We further compared the specimens from the VG160 and mVG161 group, some pathways involved were more significantly affected by VG161 (Figure 3B). This was probably caused by the expressions of exogenous genes.

3.4 | Impact of VG161 on pathways and cell type profiling of human samples

To confirm VG161 caused changes in tumor microenvironment in clinical tumor samples, seven RNA samples from two patients were tested using a Nanostring IO 360 Panel. Preinjection samples from patient 1 were of poor quality and not viable for analysis. Only one patient had both pre- and posttreatment samples. Figure 4A shows the results of a pathway score analysis, indicating that the enriched pathways associated with IFN signaling, cytotoxicity, cell apoptosis, immune cell adhesion, and cell migration were significantly activated, and the cell proliferation signal pathway was substantially suppressed. Figure 4B shows the cell type profiling results. Together, these findings validated that the main immune cells contributing the cancer-killing capcity (e.g., CD4+ and CD8+ T cells, and Dendritic cells [DCs]), were upregulated in the TME after treatment, which was in consistent with the in vivo results from pancreatic cancer mouse model.

3.5 | VG161 in combination with drugs currently in clinic

We successfully established a humanized immune system (huHSC-NOG) in NOG mice by irradiation (2.0 Gy) and tail vein injection of CD34+ human hematopoietic stem cells (HSCs). All the HSCs were collected from one human donor in Asian race. The percentage of hCD45+ cells in the peripheral blood of all enrolled mice was greater than 25% (Figure 5A). We subsequently subcutaneously implanted BxPC-3 cells in huHSC-NOG to construct a tumor model. The specific administration strategy is shown in Figure 5A.

To be noteworthy, one characteristic of OVs is that it could induce PD-L1 expression after the infection.[23] In an experiment,
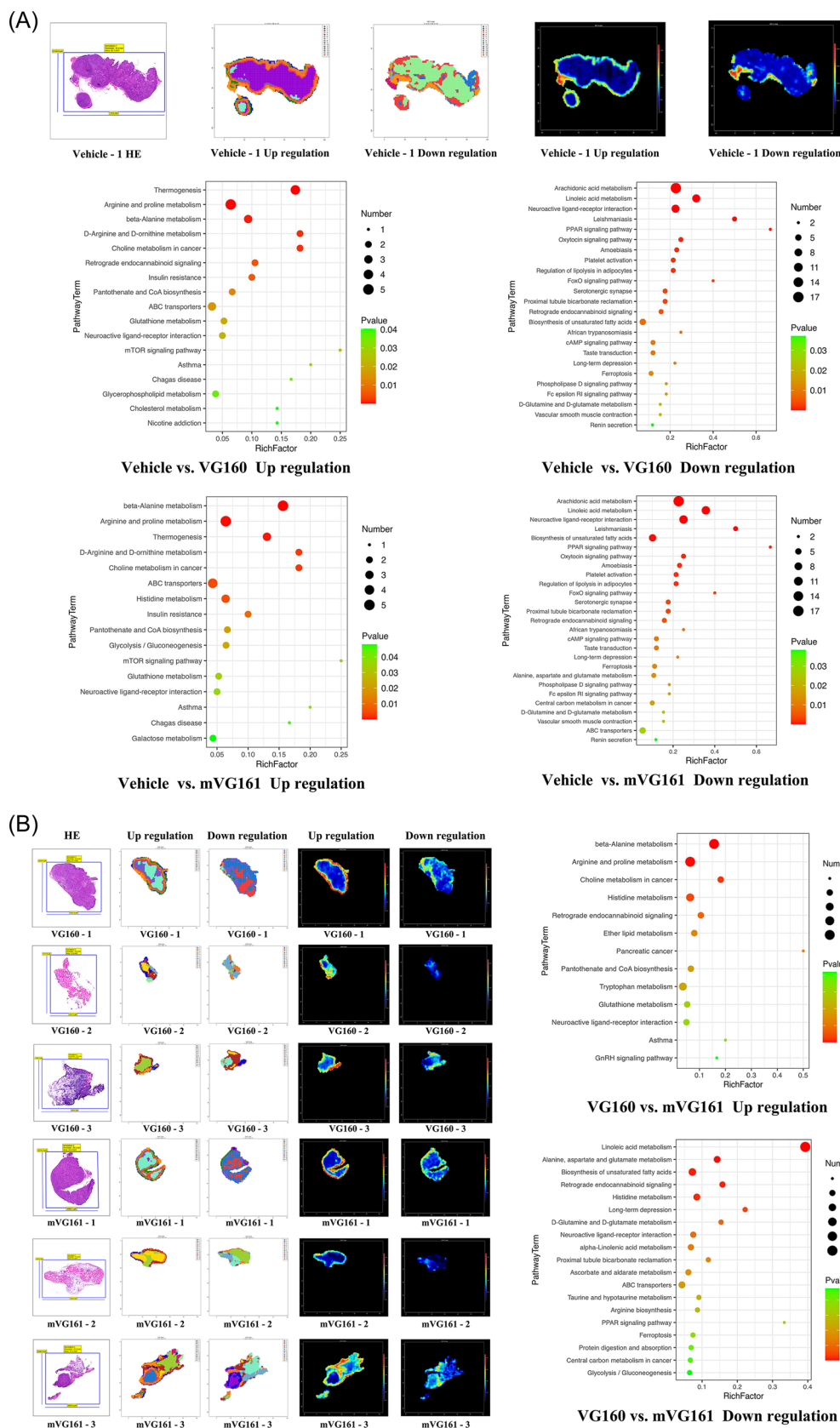
FIGURE 3 (See caption on next page)

BxPC-3 cells were infected with VG160 or VG161, and the flow cytometry results showed that the expression level of PD-L1 in the VG160 group was increased by approximately 27% compared with that of the vehicle group. In contrast, PD-L1 expression in the VG161 group was increased by only about 10% due to the action of the PD-L1 blocker (Figure 5B). In this case, a prospective way to improve the therapeutic effect of VG161 is to incorporate ICIs to combat the remaining 10% of PD-L1 expression. We selected the left tumor of the huHSC-NOG mouse model as the injection focus for injection treatment. As shown in Figure 5C, there was a significant difference in the therapeutic effect of VG161 compared with the vehicle group on the injection side. Although no significant difference between VG161 monotherapy and PD-1 monoclonal antibody therapy was observed, obvious advantages were also found. The treatment of VG161 combined with the PD-1 monoclonal antibody group was associated with a more obvious effect. In the noninjection side, the result also showed certain therapeutic advantages compared with the vehicle group when VG161 was administered as a single drug; however, this different was not significant. Significant advantages were observed following treatment with VG161 combined with PD-1 monoclonal antibody compared with the vehicle group. In addition, the expression of immune cells in peripheral blood was detected in the mice on Day 22 following VG161 administration. It demonstrated that NK cells in the PD-1 + VG161 combination group were slightly higher than other groups, meanwhile, the proportion of CD8+ T cells was significantly increased in the VG161 group and PD-1 + VG161 group (Figure 5D). Therefore, the strategy of combining PD-1 monoclonal antibody treatment with VG161 has great antitumor potential.

Since chemotherapy is the mainstream treatment for advanced pancreatic cancer, we tested the therapeutic effect of VG161 combined with Gemcitabine + Nab-Paclitaxel (GEM + Nab-PTX) chemotherapy in a nude mice model of pancreatic cancer. We first determined the optimal combination dose of VG161 in nude mice with pancreatic cancer, which was 1×10^5 PFU (Supporting Information: Figure 3). Furthermore, we established five groups, which were comprised of vehicle Group, GEM + Nab-PTX Single Drug Group, VG161 Single Drug Group, GEM + Nab-PTX First Injection VG161 Group (GEM + Nab-PTX + VG161 Group), and VG161 First Injection GEM + Nab-PTX Group (VG161 + GEM + Nab-PTX Group). The results showed that the tumor inhibitory effect of the VG161 group was superior compared to that of the GEM + Nab-PTX group. No significant difference was observed between the GEM + Nab-PTX + VG161 and VG161 groups; however, the VG161 + GEM + Nab-PTX group displayed a better therapeutic effect (Figure 6B). In terms of remission rate, the partial remission of the four

administration groups reached 100%, while the complete remission was 0% (Figure 6C). Therefore, VG161 combined with GEM + Nab-PTX chemotherapy may represent a potential treatment for advanced pancreatic cancer; however, the sequence of administration may influence the curative effect.

4 | DISCUSSION

Cytokine-armed OVs have been actively pursued as a novel treatment strategy for cancer.[24] As the first oncolytic virus carrying multiple synergistic antitumor immunostimulating factors, VG161 has been confirmed to have the capability of reconstructing the immune microenvironment in previous studies.[19] In this study, we further elucidated the specific VG161 antitumor mechanism of action in pancreatic cancer models, providing guidance for future clinical application on pancreatic cancer.

The antitumor efficacy of OVs primarily stem from the collaborative effects of direct tumor lysis, the induction of antitumor immune responses aroused by the exogenous genes and neoantigens. The results of this study show that VG161 does not have a strong tumor lysis effect. The main reason for this finding is that the construction of VG161 emphasizes the stable release of antitumor immunostimulating factors and fully activating the antitumor immune response. The purpose of IL-12 expression is to stimulate and strengthen acquired antitumor immunity.[25,26] However, in addition to reactivate the exhausted or anergic T cells, IL-15 has been demonstrated to promote the production of both CD8+ T cells and NK cells and can synergistically interact with IL-12.[27] A PD-L1 blocker is equivalent to an ICI, which can improve the immunosuppressive microenvironment of a tumor. In theory, these antitumor immunostimulating factors can act on every facet of CIC and CNIC, and fully amplify the antitumor immune response. By single-cell sequencing analysis on mouse pancreatic cancer tissues, we found that VG161 can induce a greater number of monocytes, T cells, and NK cell infiltration into tumor tissues compared with VG160. In addition, the proportion of Tregs is also reduced. Therefore, the exogenous gene carried by VG161 does play a positive role in antitumor immunity. One limitation is that single-cell sequencing on the uninjected lesions was not performed. We believe that the uninjected lesions were not infected with the virus, and its immune microenvironment changes more naturally. Compared with VG160, the influence of VG161 on the immune microenvironment of the uninjected lesions should be more obvious. Due to technical reasons, the level of VG161 exogenous gene expression, especially IL-15/IL-15Rα, appears to be less than ideal, which also affects its ability to

FIGURE 3 The mouse subcutaneous tumor samples represent clear differences in the metabolic microenvironment following treatment with VG160 or VG161. Pretreatment (vehicle) and posttreatment (VG160 or VG161) subcutaneous tumor samples isolated from mice show clear differences in the metabolic microenvironment by airflow-assisted desorption electrospray ionization-mass spectrometry imaging (AFADSI-MSI). (A) AFADSI-MSI analysis of metabolic microenvironment from isolated subcutaneous tumor samples (vehicle vs. VG160 or VG161). (B) The bubble diagram of upregulated pathways and downregulated pathways. Composition of vehicle: 50 mM Tris-HCl, 150 mM NaCl, 5% glycerol.
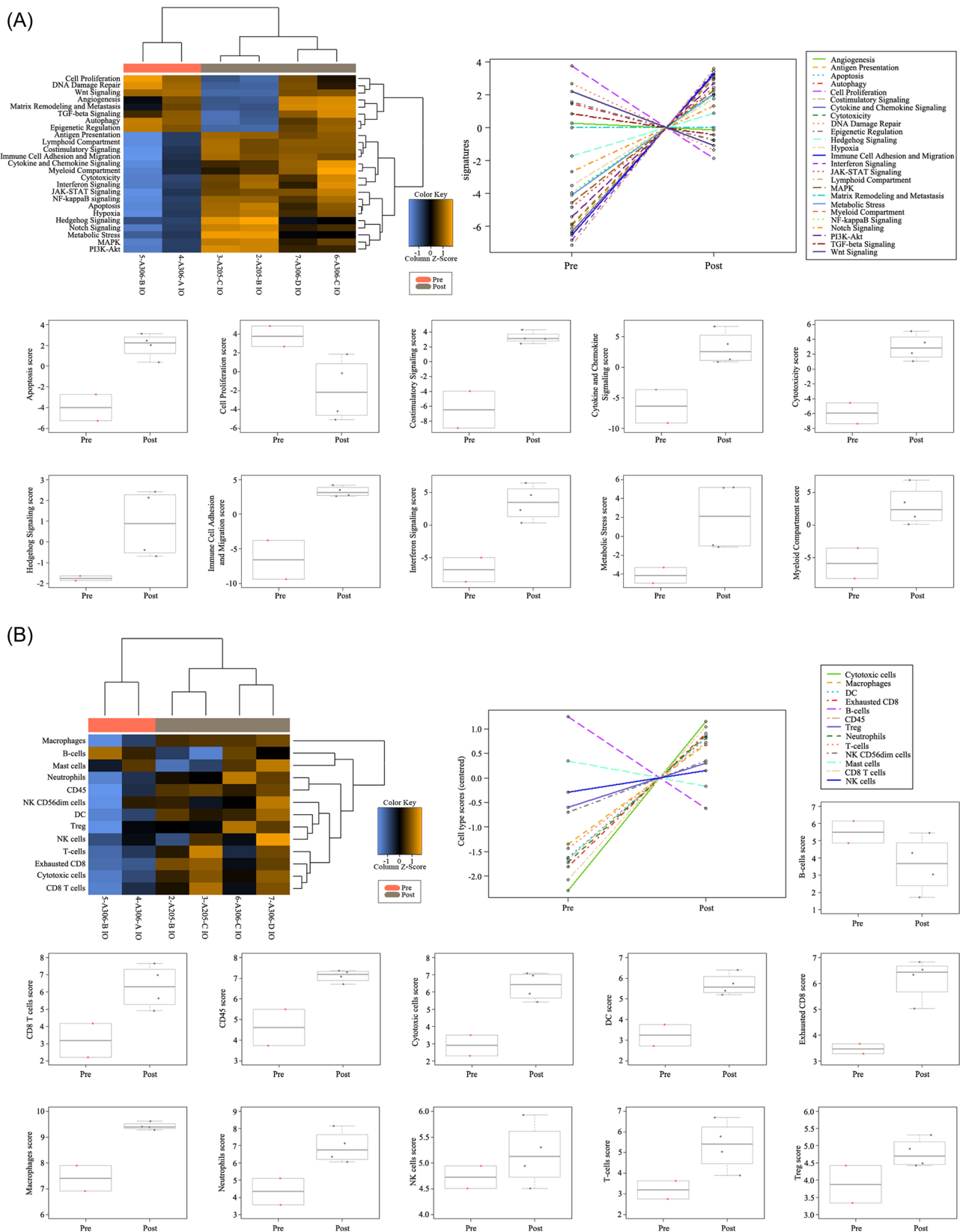
FIGURE 4 Pretreatment and posttreatment human tumor samples demonstrate clear differences in the nanostring analysis. Patient from Australia participated in Phase I clinical trial for investigational new drug VG161. (A) Pathway score analysis. (B) Cell type profiling.
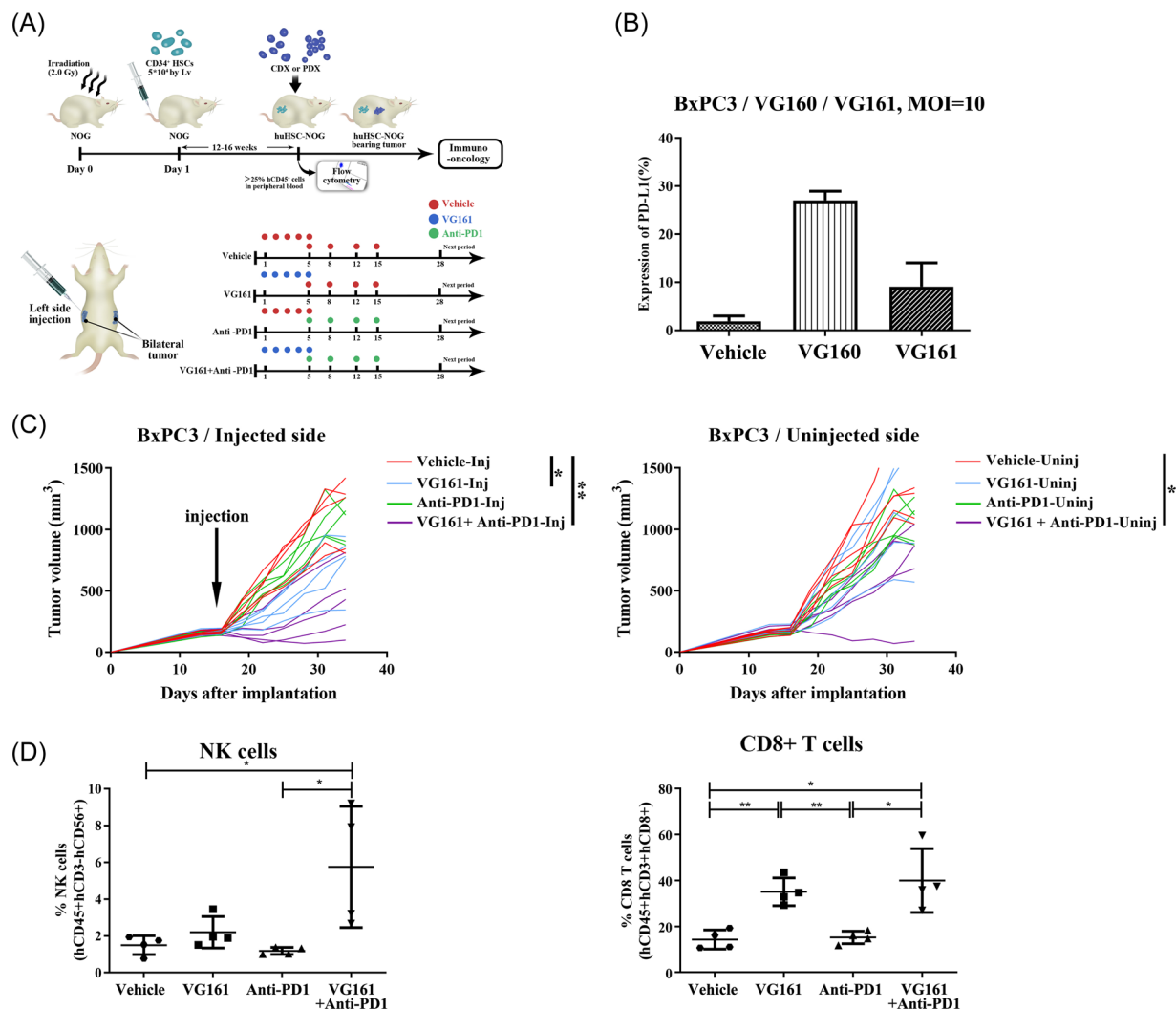
FIGURE 5 In the humanized mouse model, the combination of VG161 and an immune checkpoint inhibitor can further enhance the ability to inhibit tumor growth. (A) Construction procedure of a humanized mouse model (huHSC-NOG mice). 5.0×10^6 BxPC-3 tumor cells were inoculated into 40 huHSC-NOG mice with more than 25% hCD45+ at the subcutaneous sites on both sides of the scapula. Thirteen days after tumor inoculation, when the average tumor volume of 40 tumor-bearing mice reached 150 mm³, the mice with a tumor volume that was too small or too large were eliminated, and the remaining 20 mice were randomly divided into four groups according to tumor volume, including the vehicle group, VG161 group (1.0×10^7 PFU/mouse), anti-1PD-1 group (10 mg/kg), and VG161 (1.0×10^7 PFU/mouse) combined with anti-PD-1 (10 mg/kg). (B) The level of PD-L1 expression on the surface of BxPC-3 cells after VG160 or VG161 infection at 48 hpi. (C) Tumor size of individual injected tumors compared to uninjected distant tumors. (D) Immune cells in peripheral blood was assessed by flow cytometry in all groups. Composition of vehicle: 50mM Tris-HCl, 150 mM NaCl, 5% glycerol. Data are shown as the mean ± SEM. Stats: Data were analyzed using an unpaired Student's t-test, $*p < 0.05$; $**p < 0.01$; $***p < 0.001$.

recruit NK cells. In this study, after VG161 treatment, the number of NK cells in the tumor tissue and peripheral blood of immune healthy mice was slightly higher than that of VG160 group; however, this difference was not significant. There is still room for VG161 to be improved and promoted (e.g., reconstructing the virus backbone to improve its replication ability and improve exogenous gene expression).

The results of this study suggest that VG161 mainly induces CD8+ T cell production to exert an antitumor immune response, especially in abscopal noninjected lesions. In both the C57BL/6 and huHSC-NOG pancreatic cancer mouse models, an obvious "abscopal

effect" was observed (i.e., the uninjected tumor was significantly inhibited under the influence of VG161). Figure 1H shows that the amount of virus in the uninjected lesions at the different time points was extremely small. Therefore, we can rule out the transmission of VG161 to uninjected lesions through the blood and its role in direct tumor lysis. On the other hand, we detected a significantly higher number of CD8+ T cells compared to those in the vehicle group in both injected and uninjected lesions by flow cytometry, particularly at Day 7 (Figure 2) following the administration. Moreover, the CD8+ T cell content in the uninjected lesions was also slightly higher than that in the injected lesions. One possible reason for this
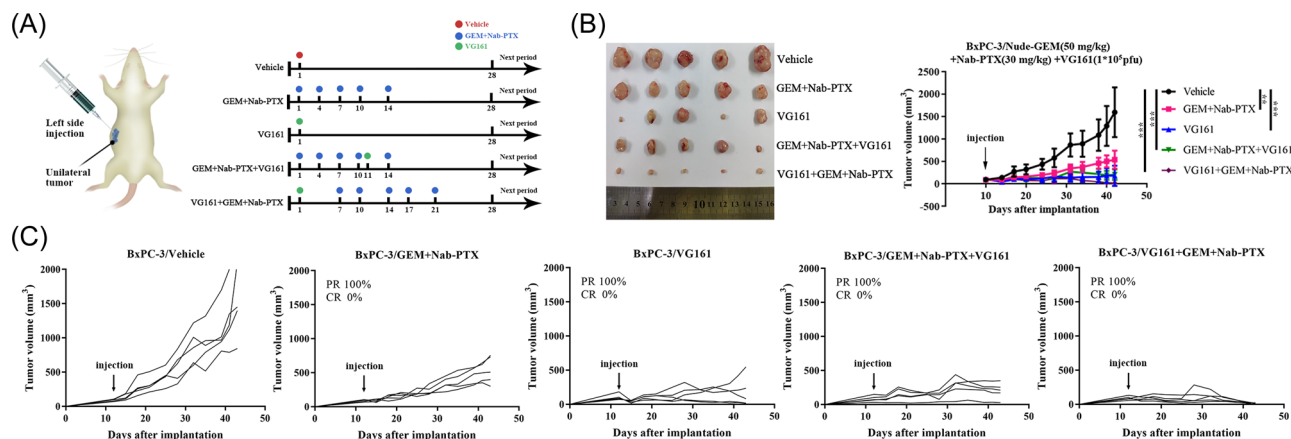
FIGURE 6 Treatment with VG161 combined with chemotherapy could further enhance the ability to inhibit tumor growth in a nude mouse model. (A) Five nude mice per group were subcutaneously implanted with 2×10^6 BxPC3 human pancreatic cancer cells into the lower left flank. When the average tumor volume of the mice reached 150 mm³, mice with a tumor volume that was either too small or too large were removed, and the remaining 25 mice were randomly divided into five groups according to the tumor volume, including the vehicle group, VG161 (1.0×10^7 PFU/mouse) group, GEM (50 mg/kg) + Nab-PTX (30 mg/kg) group, GEM + Nab-PTX + VG161 combined treatment group, and VG161 + GEM + Nab-PTX combined treatment group. (B) Growth of injected tumors. (C) Tumor size of individual injected tumors (right). Quantification of Tumor size at indicated time points (left). Composition of vehicle: 50 mM Tris-HCl, 150 mM NaCl, 5% glycerol. Data are presented as the mean ± SEM. Stats: Data were analyzed using an unpaired Student's t-test, $*p < 0.05$; $**p < 0.01$; $***p < 0.001$.

observation is that the tumor immune microenvironment of the noninjected lesions occurs more naturally because it was not infected with the virus. In contrast, the tumor focus on the injected side stimulates negative immune regulation as a result of the virus infection.[23,28] Interestingly, in the current ongoing Phase I clinical trial, VG161 has also shown abscopal effects in noninjected lesions in patients.[29] In addition, in the Nanostring results, multiple immune-related cell types were observed, including the upregulation of CD4, CD8, and DCs in the tumor microenvironment. Together with the differential gene expression data, VG161 treatment can heat up the tumor and generate additional immunoactivity in the tumor microenvironment.

ICIs are natural synergists of OVs. As mentioned above, OV infection of tumor cells would cause increased level of PD-L1 expression on the tumor surface, possibly promoting Treg upregulation in TME and cytotoxic T lymphocyte-associated protein 4 (CTLA4) expression on the T cell surface.[23,28] Moreover, ICIs can combat the negative effects of such immunosuppression. A phase 1b clinical trial tested the impact of oncolytic virotherapy with T-VEC on cytotoxic T cell infiltration and therapeutic efficacy of the anti-PD-1 antibody, pembrolizumab.[11] The results show that the confirmed objective response rate was 62%, with a complete response rate of 33% per immune-related response criteria. In our research, the cell surface expression of PD-L1 on BxPC-3 increased by approximately 27% after the infection of VG160. While the PD-L1 blocker delivered by VG161 could prevent PD-L1 upregulation to some extent, however, there still existed PD-L1 that hindered an optimal curative outcome of VG161. Theoretically, the PD-1/PD-L1 monoclonal antibody would be an ideal synergistic drug to VG161. In the huHSC-NOG pancreatic cancer mouse model, we successfully confirmed that the combination therapy of anti-PD-1 mAb and VG161 deliver the

optimal therapeutic performance. Therefore, a clinical study of the use of VG161 in combination with nivolumab in subjects with advanced pancreatic cancer will be performed at our center.

Chemotherapy is the most important treatment for advanced pancreatic cancer. Here, we explored the pharmacodynamics of VG161 used in combination with GEM + Nab-PTX in a mouse model of pancreatic cancer. The results showed that the combination scheme exhibited certain advantages over treatment with a single drug. More importantly, differences in the curative effect were observed under different administration sequences. It is generally believed that chemotherapy drugs can improve the tumor micro-environment while killing tumor cells, resisting tumor immune escape mechanisms, and provide a "hotbed" for immune antitumor drugs to play their role.[30–34] Therefore, the use of chemotherapeutic drugs followed by VG161 can theoretically optimize the outcome. In our study, it is found that VG161 followed by chemotherapy was associated with the optimal effect. We believe that although OVs are a type of immunological antitumor drug, effective viral replication is the premise of its function. After the initial use of chemotherapy drugs, a large number of tumor cells died, which prohibited the OVs from relying upon active tumor cells to replicate, leading to the above results. The deficiency of this study is that we only carried out this experiment in a pancreatic cancer model using nude mice with immunodeficiency. Thus, our inference cannot be completely confirmed in the absence of acquired immune cells. Further research is worth investigating.

In the past decades, the issue that whether OVs participate in regulating tumor metabolisms has rarely been studied. Therefore, we performed preliminarily metabolic analysis in pancreatic cancer mouse model after receiving the treatment with OVs in this study. Conformed to our speculations, distinctive changes in metabolic

pathways were observed following the VG160 or the VG161 treatment. We will further explore the relationship between OVs and tumor metabolism in future studies and seek sensitive metabolic OV markers so as to expand the application of OVs.

In conclusion, we found that VG161 could exert its antitumor effect by reconstructing the tumor immune microenvironment in pancreatic cancer mouse models. At the cellular level, the killing activities would be contributed to the upregulated CD8+ T cell and NK cell populations elicited by the VG161 treatment. The strategy of combining VG161 with ICIs for pancreatic cancer has great potential. The combination of VG161 and chemotherapy is also worth testing; however, but the sequence for treatment delivery requires further exploration. Therefore, the anticancer strategy of VG161 administered alone or in combination with other therapies deserves further exploration in clinical trials.

AUTHOR CONTRIBUTIONS

ACKNOWLEDGMENT

CONFLICT OF INTEREST

The authors declare no conflict of interest.

DATA AVAILABILITY STATEMENT

The data that support the findings of this study are available from the corresponding author upon reasonable request.

ETHICS STATEMENT

Tumor samples was obtained from a Phase 1 clinical trial (ACTRN12620000244909) conducted at the Kinghorn Cancer Center in Australia. All patients provided signed informed consent according to guidelines. Consent forms and protocols were approved by the Australia Therapeutic Goods Administration, the Institutional Review and Ethics Committee at the hospital. Animal experiments were performed with the approval of the Tab of Animal Experimental Ethical Inspection of the First Affiliated Hospital, College of Medicine, Zhejiang University.

ORCID

Yuwei Li http://orcid.org/0000-0002-9290-6701

REFERENCES

1. Amundadottir LT. Pancreatic cancer genetics. *Int J Biol Sci.* 2016;12(3):314-325.
2. Chiaravalli M, Reni M, O'Reilly EM. Pancreatic ductal adenocarcinoma: state-of-the-art 2017 and new therapeutic strategies. *Cancer Treat Rev.* 2017;60:32-43.
3. Kelly E, Russell SJ. History of oncolytic viruses: genesis to genetic engineering. *Mol Ther.* 2007;15(4):651-659.
4. Lawler SE, Speranza MC, Cho CF, Chiocca EA. Oncolytic viruses in cancer treatment: a review. *JAMA Oncol.* 2017;3(6):841-849.
5. Li Y, Shen Y, Zhao R, et al. Oncolytic virotherapy in hepato-biliopancreatic cancer: the key to breaking the log jam? *Cancer Med.* 2020;9(9):2943-59.
6. Andtbacka RH, Kaufman HL, Collichio F, et al. Talimogene laherparepvec improves durable response rate in patients with advanced melanoma. *J Clin Oncol.* 2015;33(25):2780-2788.
7. Andtbacka RHI, Collichio F, Harrington KJ, et al. Final analyses of OPTiM: a randomized phase III trial of talimogene laherparepvec versus granulocyte-macrophage colony-stimulating factor in unresectable stage III-IV melanoma. *J Immunother Cancer.* 2019;7(1):145.
8. Chesney J, Awasthi S, Curti B, et al. Phase IIIb safety results from an expanded-access protocol of talimogene laherparepvec for patients with unresected, stage IIIB-IVM1c melanoma. *Melanoma Res.* 2018;28(1):44-51.
9. Hu JC, Coffin RS, Davis CJ, et al. A phase I study of OncoVEXGM-CSF, a second-generation oncolytic herpes simplex virus expressing granulocyte macrophage colony-stimulating factor. *Clin Cancer Res.* 2006;12(22):6737-6747.
10. Liu BL, Robinson M, Han ZQ, et al. ICP34.5 deleted herpes simplex virus with enhanced oncolytic, immune stimulating, and anti-tumour properties. *Gene Ther.* 2003;10(4):292-303.
11. Ribas A, Dummer R, Puzanov I, et al. Oncolytic virotherapy promotes intratumoral T cell infiltration and improves anti-PD-1 immunotherapy. *Cell.* 2017;170(6):1109-1119.e10.
12. Beury DW, Parker KH, Nyandjo M, Sinha P, Carter KA, Ostrand-Rosenberg S. Cross-talk among myeloid-derived suppressor cells, macrophages, and tumor cells impacts the inflammatory milieu of solid tumors. *J Leukoc Biol.* 2014;96(6):1109-1118.
13. Clive KS, Tyler JA, Clifton GT, et al. Use of GM-CSF as an adjuvant with cancer vaccines: beneficial or detrimental? *Expert Rev Vaccines.* 2010;9(5):519-525.
14. Wada S, Jackson CM, Yoshimura K, et al. Sequencing CTLA-4 blockade with cell-based immunotherapy for prostate cancer. *J Transl Med.* 2013;11:89.
15. Chen DS, Mellman I. Oncology meets immunology: the cancer-immunity cycle. *Immunity.* 2013;39(1):1-10.
16. Huntington ND, Cursons J, Rautela J. The cancer-natural killer cell immunity cycle. *Nat Rev Cancer.* 2020;20(8):437-54.
17. Hamid O, Robert C, Daud A, et al. Safety and tumor responses with lambrolizumab (anti-PD-1) in melanoma. *N Engl J Med.* 2013;369(2):134-144.
18. Corbière V, Chapiro J, Stroobant V, et al. Antigen spreading contributes to MAGE vaccination-induced regression of melanoma metastases. *Cancer Res.* 2011;71(4):1253-1262.
19. Chouljenko DV, Ding J, Lee IF, et al. Induction of durable antitumor response by a novel oncolytic herpesvirus expressing multiple immunomodulatory transgenes. *Biomedicines.* 2020;8(11):484.
20. Rivadeneira DB, DePeaux K, Wang Y, et al. Oncolytic viruses engineered to enforce leptin expression reprogram tumor-infiltrating T cell metabolism and promote tumor clearance. *Immunity.* 2019;51(3):548-560.e4.

21. Zhang B, Wang X, Cheng P. Remodeling of tumor immune micro-environment by oncolytic viruses. *Front Oncol.* 2020;10:561372.

22. Ravirala D, Pei G, Zhao a, Zhang X. Comprehensive characterization of tumor immune landscape following oncolytic virotherapy by single-cell RNA sequencing. *Cancer Immunol Immunother.* 2022;71(6):1479-1495.

23. Chaurasiya S, Yang A, Kang S, et al. Oncolytic poxvirus CF33-hNIS-DeltaF14.5 favorably modulates tumor immune microenvironment and works synergistically with anti-PD-L1 antibody in a triple-negative breast cancer model. *Oncoimmunology.* 2020;9(1):1729300.

24. Chen T, Ding X, Liao Q, et al. IL-21 arming potentiates the anti-tumor activity of an oncolytic vaccinia virus in monotherapy and combination therapy. *J Immunother Cancer.* 2021;9(1):e001647.

25. Tugues S, Burkhard SH, Ohs I, et al. New insights into IL-12-mediated tumor suppression. *Cell Death Differ.* 2015;22(2):237-246.

26. Wigginton JM, Wiltrout RH. IL-12/IL-2 combination cytokine therapy for solid tumours: translation from bench to bedside. *Expert Opin Biol Ther.* 2002;2(5):513-524.

27. Robinson TO, Schluns KS. The potential and promise of IL-15 in immuno-oncogenic therapies. *Immunol Lett.* 2017;190:159-68.

28. Noonan AM, Farren MR, Geyer SM, et al. Randomized phase 2 trial of the oncolytic virus pelareorep (reolysin) in upfront treatment of metastatic pancreatic adenocarcinoma. *Mol Ther.* 2016;24(6):1150-1158.

29. Zhao R, Cosman R, Aggarwal N, et al. Initial results from a first in human trial incorporating accelerated dose titration of a novel immune stimulating oncolytic virus—VG161. *J Clin Oncol 39.* 2021;suppl 15:abstre14574.

30. Adair SJ, Hogan KT. Treatment of ovarian cancer cell lines with 5-aza-2'-deoxycytidine upregulates the expression of cancer-testis antigens and class I major histocompatibility complex-encoded molecules. *Cancer Immunol Immunother.* 2009;58(4):589-601.

31. Armeanu S, Krusch M, Baltz KM, et al. Direct and natural killer cell-mediated antitumor effects of low-dose bortezomib in hepato-cellular carcinoma. *Clin Cancer Res.* 2008;14(11):3520-3528.

32. Liu WM, Fowler DW, Smith P, Dalgleish AG. Pre-treatment with chemotherapy can enhance the antigenicity and immunogenicity of tumours by promoting adaptive immune responses. *Br J Cancer.* 2010;102(1):115-123.

33. Ma Y, Adjemian S, Mattarollo SR, et al. Anticancer chemotherapy-induced intratumoral recruitment and differentiation of antigen-presenting cells. *Immunity.* 2013;38(4):729-741.

34. Spisek R, Charalambous A, Mazumder A, Vesole DH, Jagannath S, Dhodapkar MV. Bortezomib enhances dendritic cell (DC)-mediated induction of immunity to human myeloma via exposure of cell surface heat shock protein 90 on dying tumor cells: therapeutic implications. *Blood.* 2007;109(11):4839-4845.

SUPPORTING INFORMATION

Additional supporting information can be found online in the Supporting Information section at the end of this article.